CRISPR

RNA-triggered protein cleavage and cell growth arrest by the type III-E CRISPR nuclease-protease

Kazuki Kato[1]†, Sae Okazaki[1]†, Cian Schmitt-Ulms[2]†, Kaiyi Jiang[2,3]†, Wenyuan Zhou[2], Junichiro Ishikawa[1], Yukari Isayama[1], Shungo Adachi[4], Tomohiro Nishizawa[5], Kira S. Makarova[6], Eugene V. Koonin[6], Omar O. Abudayyeh[2]*, Jonathan S. Gootenberg[2]*, Hiroshi Nishimasu[1,7,8,9]*

The type III-E CRISPR–Cas7-11 effector binds a CRISPR RNA (crRNA) and the putative protease Csx29 and catalyzes crRNA-guided RNA cleavage. We report cryo–electron microscopy structures of the Cas7-11–crRNA–Csx29 complex with and without target RNA (tgRNA), and demonstrate that tgRNA binding induces conformational changes in Csx29. Biochemical experiments revealed tgRNA-dependent cleavage of the accessory protein Csx30 by Csx29. Reconstitution of the system in bacteria showed that Csx30 cleavage yields toxic protein fragments that cause growth arrest, which is regulated by Csx31. Csx30 binds Csx31 and the associated sigma factor RpoE (RNA polymerase, extracytoplasmic E), suggesting that Csx30-mediated RpoE inhibition modulates the cellular response to infection. We engineered the Cas7-11–Csx29–Csx30 system for programmable RNA sensing in mammalian cells. Overall, the Cas7-11–Csx29 effector is an RNA-dependent nuclease-protease.

Prokaryotic CRISPR-Cas systems provide adaptive immunity against foreign nucleic acids, including phages and mobile genetic elements, through diverse mechanisms of programmed nucleic acid cleavage. CRISPR-Cas systems are divided into two classes based on the number of components in the effector complexes responsible for defense through the cleavage of invading nucleic acids programmed by a CRISPR RNA (crRNA) guide (*1*, *2*). In class 1 systems, which encompass types I, III, and IV, target nucleic acids are degraded by multiprotein effector complexes, whereas the effectors of class 2 systems (types II, V, and VI) are single-protein, multidomain Cas proteins (Cas9, Cas12, and Cas13, respectively). CRISPR-Cas systems also deploy a wide array of accessory proteins that enhance and modulate the antiviral activity of the primary effector nuclease (*3*–*7*).

Unlike typical class 1 effectors, the type III-E effector Cas7-11 (also known as gRAMP) is a single-protein, multidomain effector that consists of four Cas7 domains (Cas7.1 to Cas7.4) and a Cas11 domain (*8*, *9*). Cas7-11 associates with a crRNA and cleaves complementary single-stranded RNA (ssRNA) targets at two defined positions using the Cas7.2 and Cas7.3 domains. Whereas the type VI effector Cas13 displays promiscuous RNase activity (*10*, *11*), Cas7-11 exhibits precise, guide RNA–dependent tgRNA cleavage activity in human cells and has been used as a new RNA-targeting tool with high specificity and low cell toxicity (*8*, *9*). The type III-E locus encodes multiple conserved accessory proteins, including Csx29 (a caspase-like putative protease with fused TPR and CHAT domains), Csx30 and Csx31 (proteins with unknown functions), and RpoE (an alternative sigma factor). Cas7-11 forms a complex with Csx29 (*8*, *9*), suggesting a potential mechanism of RNA-guided protease activity for antiviral immunity. Recently, we reported the cryo–electron microscopy (cryo-EM) structure of *Desulfonema ishimotonii* Cas7-11 complexed with its cognate crRNA and tgRNA (*12*), providing mechanistic insights into pre-crRNA processing and tgRNA cleavage. Nonetheless, the means by which Cas7-11 cooperates with the other proteins encoded in the type III-E locus (Csx29, Csx30, Csx31, and RpoE) and binds Csx29 to potentially activate its protease activity remain unknown.

Results

Structures of Cas7-11 complexed with Csx29

We sought to solve the structure of the Cas7-11–Csx29 effector complex to gain insights into its action mechanism. We coexpressed the catalytically inactive *D. ishimotonii* Cas7-11 mutant (referred to as Cas7-11 for simplicity), with the D429A (Cas7.2) and D654A (Cas7.3) mutations introduced to prevent tgRNA cleavage by Cas7-11, together with Csx29 and a crRNA transcribed from a CRISPR array containing two repeat-spacer units and then purified the Cas7-11–crRNA–Csx29 complex. We determined cryo-EM structures of this Cas7-11–crRNA–Csx29 complex with and without a tgRNA at 2.5- and 2.8-Å resolutions, respectively (Fig. 1, A to D, figs. S1 to S3, table S1, and movie S1). In both structures, Cas7-11 adopts a modular architecture consisting of four Cas7 domains (Cas7.1 to Cas7.4) with a zinc finger (ZF) motif, a Cas11 domain, an insertion (INS) domain within the Cas7.4 domain, a C-terminal extension domain, and four interdomain linkers (L1 to L4) (Fig. 1, C and D), as in the Csx29-unbound Cas7-11–crRNA–tgRNA structure (*12*) (fig. S4).

The 15-nucleotide (nt) 5′ tag region [U(−15)–C(−1)] in the 38-nt crRNA [U(−15)–A23] is anchored by the Cas7.1 and Cas7.2 domains in both structures (Fig. 1, C and D, and figs. S4, B and C, and S5A), as in the Csx29-unbound Cas7-11–crRNA–tgRNA structure (*12*) (fig. S4A). The 23-nt crRNA spacer region is recognized by the Cas7.2 to Cas7.4 domains in the tgRNA-free structure (Fig. 1C and fig. S4B), whereas the crRNA spacer region (C1 to A23, except for U4 and C10) hybridizes with the tgRNA (G1 to U23, except for A4 and G10) to form a guide-target duplex in the tgRNA-bound structure (Fig. 1D and fig. S4C). A(−3) in the 5′ tag (6 nt downstream of the first flipped-out spacer nucleotide) is flipped out because of its interaction with the thumb-like β-hairpin in the Cas7.1 domain (fig. S5B), similar to the equivalent nucleotide C(−1) in the type III-A Csm effector complex (*13*, *14*) (fig. S5C). Nonetheless, unlike the Csm complex, A(−2) and C(−1), which are located upstream of A(−3), cannot base pair with the tgRNA in Cas7-11 because of the presence of the L2 linker (fig. S5B), explaining the distinct RNA cleavage patterns between the Cas7-11 and Csm effector complexes. In the present structures, the peripheral region (residues 1043 to 1124) of the INS domain was less resolved in the density map, probably because of its flexibility (fig. S3), and was excluded from the final models (fig. S4).

Csx29 structure

Csx29 consists of a tetratricopeptide repeat (TRP) domain (residues 1 to 422) and a Caspase HetF Associated with TPRs (CHAT) protease domain (residues 423 to 751) (Fig. 2A). The TRP domain can be divided into an N-terminal domain (NTD) (residues 1 to 64), seven TPR units (TPR1 to TPR7), and a central region referred to as the activation region (AR). The NTD adopts a three-helix bundle structure and interacts with the Cas7.4 domain of Cas7-11 (Fig. 2B). In Csx29, each TPR unit contains two α helices, similar to canonical TPR-containing proteins in which the TPRs interact with their protein targets (*15*). Correspondingly, TPR1 and TPR2 of Csx29 interact with the L2 linker of

[1]Structural Biology Division, Research Center for Advanced Science and Technology, The University of Tokyo, 4-6-1 Komaba, Meguro-ku, Tokyo 153-8904, Japan. [2]McGovern Institute for Brain Research at MIT, Massachusetts Institute of Technology, Cambridge, MA 02139, USA. [3]Department of Biological Engineering, Massachusetts Institute of Technology, Cambridge, MA 02139, USA. [4]Cellular and Molecular Biotechnology Research Institute, National Institute of Advanced Industrial Science and Technology, 2-4-7 Aomi, Koto-ku, Tokyo 135-0064, Japan. [5]Graduate School of Medical Life Science, Yokohama City University, 22-2 Seto, Kanazawa-ku, Yokohama, Kanagawa 236-0027, Japan. [6]National Center for Biotechnology Information, National Library of Medicine, National Institutes of Health, Bethesda, MD 20894, USA. [7]Department of Chemistry and Biotechnology, Graduate School of Engineering, The University of Tokyo, 7-3-1 Hongo, Bunkyo-ku, Tokyo 113-8656, Japan. [8]Department of Biological Sciences, Graduate School of Science, The University of Tokyo, 7-3-1 Hongo, Bunkyo-ku, Tokyo 113-0033, Japan. [9]Inamori Research Institute for Science, 620 Suiginya-cho, Shimogyo-ku, Kyoto 600-8411, Japan.
*Corresponding author. Email: omar@abudayyeh.science (O.O.A.); jgoot@mit.edu (J.S.G.); nisimasu@g.ecc.u-tokyo.ac.jp (H.N.)
†These authors contributed equally to this work.

Downloaded from https://www.science.org at Shanghai Normal University on November 25, 2022

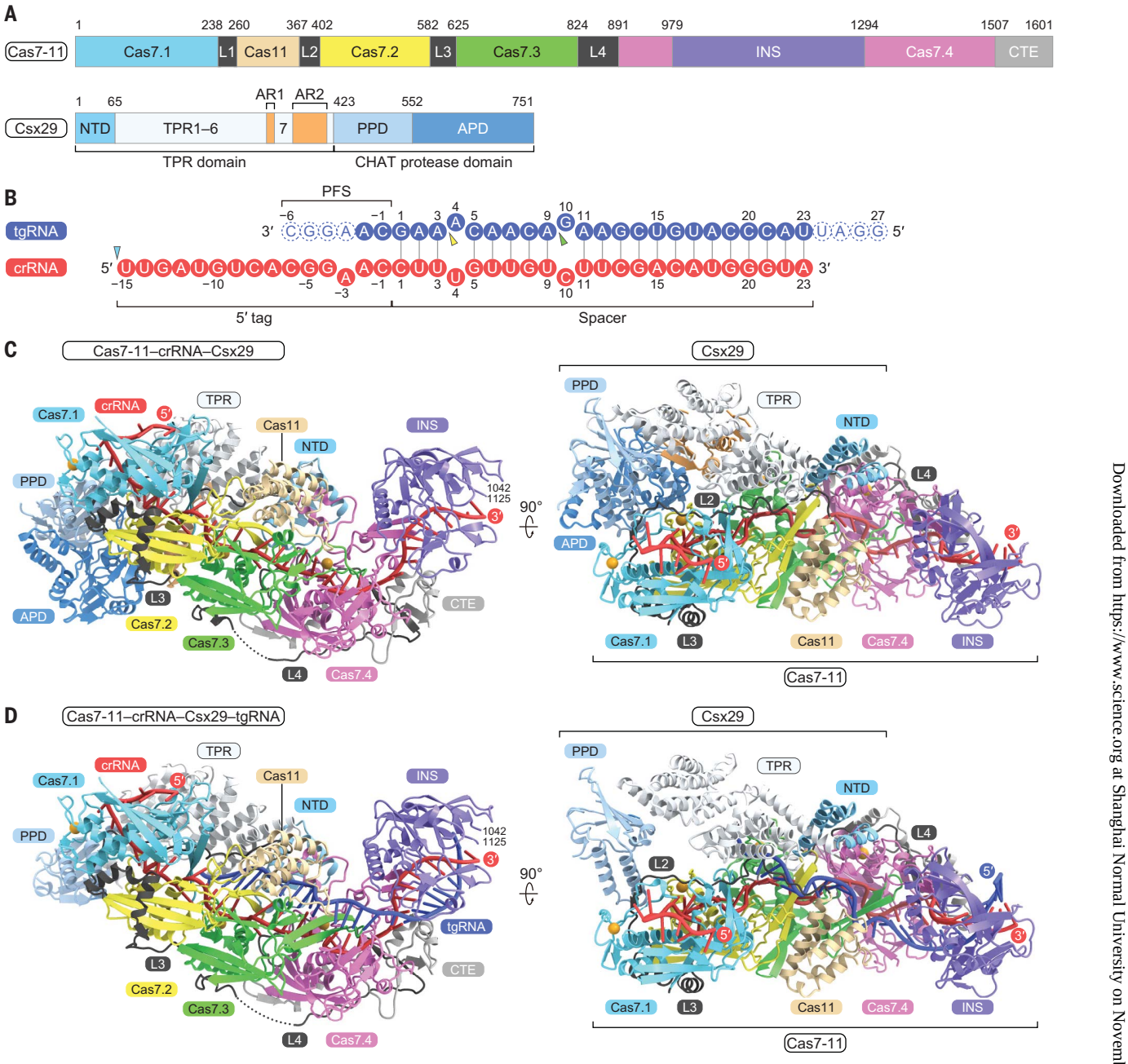


Fig. 1. Cryo-EM structures of the Cas7-11–crRNA–Csx29 complexes with and without the tgRNA. (**A**) Domain structures of Cas7-11 and Csx29. (**B**) Nucleotide sequences of the crRNA and its tgRNA. The pre-crRNA processing site and the tgRNA cleavage sites are indicated by cyan and yellow/green triangles, respectively. Disordered nucleotides are indicated by dotted lines. (**C** and **D**) Overall structures of Cas7-11–crRNA–Csx29 (C) and Cas7-11–crRNA–Csx29–tgRNA (D). The bound zinc ions are shown as orange spheres. The disordered L1 and L2 linkers are not shown for clarity. PPD, pseudo-protease domain.

Cas7-11 (Fig. 2B). The CHAT domain of Csx29 consists of a central 11-stranded mixed β-sheet and flanking α-helices, and can be divided into a pseudo-protease domain (residues 423 to 551) and an active-protease domain (APD) (residues 552 to 751) with the conserved putative catalytic residues H615 and C658 (Fig. 2A). A Dali search (*16*) confirmed that the CHAT domain of Csx29 structurally resembles caspase-like cysteine proteases such as human separase (*17*) (fig. S6). In the Cas7-11–crRNA–Csx29 structure, the AR consists of two regions, AR1 (a β-hairpin between TPR6 and TPR7) and AR2 (a β-strand and a helix-loop-helix after TPR7), and interacts with TPR1–TPR6 and the APD (Fig. 2A).

Interactions between Cas7-11 and Csx29

In the Cas7-11–crRNA–Csx29 structure, Csx29 interacts with multiple regions of Cas7-11 (Fig. 2B and fig. S7A). The L2 linker (residues 367 to 401) and α-helical insertion (residues 1313 to 1341) in the Cas7.4 ZF motif, which are disordered in the Csx29-unbound Cas7-11 structure (*12*) (fig. S7B), are ordered and form interactions with Csx29 in the Cas7-11–crRNA–Csx29 structure (Fig. 2B and fig. S7, C and D). This α-helical insertion in the ZF motif is unique to Cas7.4 (fig. S7C). The NTD of Csx29 mainly interacts with the Cas7.4 domain of Cas7-11 (Fig. 2B and figs. S7A and S8A). In addition, the Cas7.2 thumb-like β-hairpin and the L2/L4 linkers reinforce the binding to the Csx29 NTD (Fig. 2B and fig. S8, B and C).

TPR1 and TPR2 interact with Cas7.3 (ZF) and L2 of Cas7-11 (Fig. 2B and figs. S7A and S8D). TPR2 also interacts with Cas7.1 (thumb-like

Downloaded from https://www.science.org at Shanghai Normal University on November 25, 2022

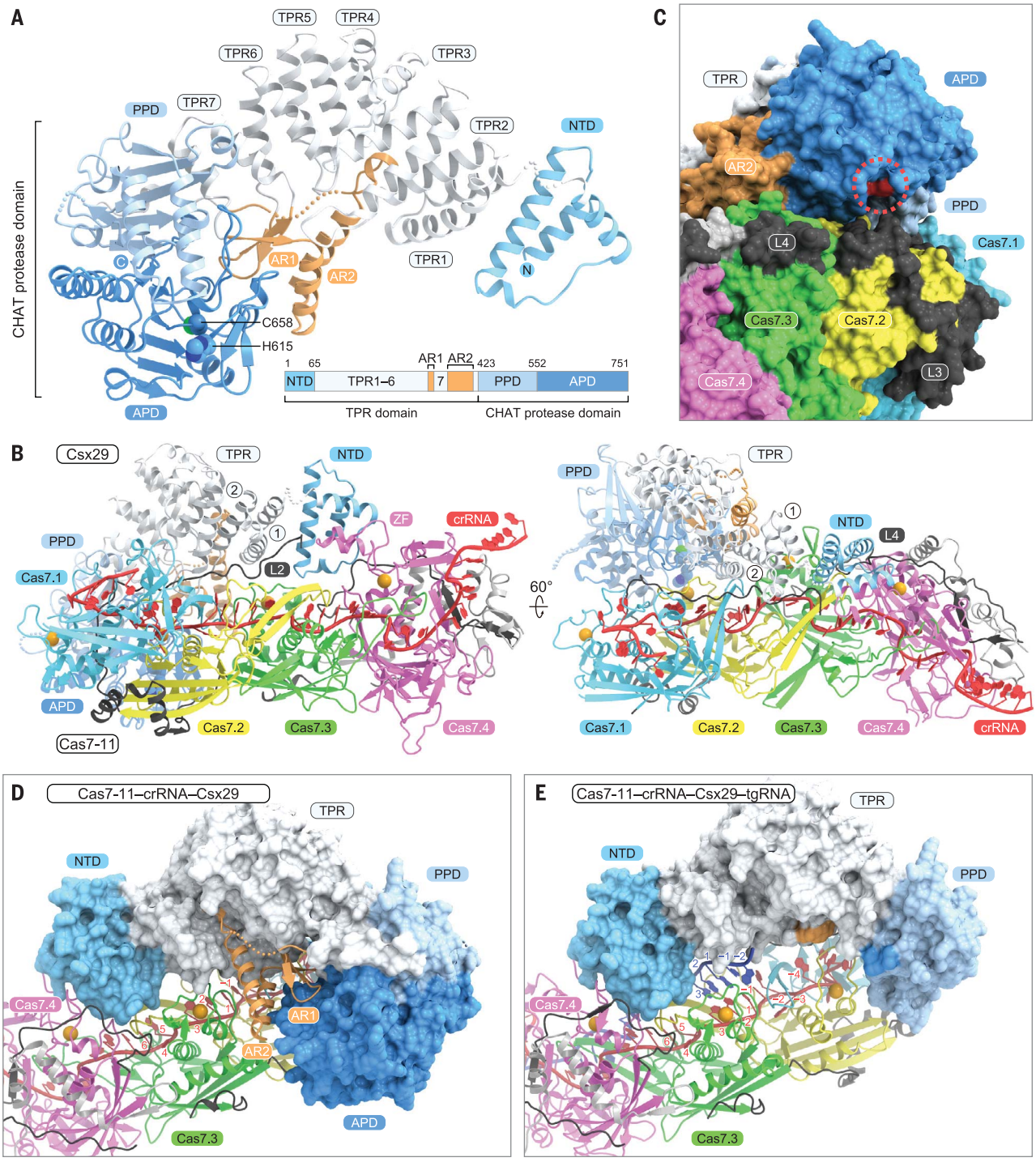


Fig. 2. Interaction between Cas7-11 and Csx29. (**A**) Structure of Csx29 in the Cas7-11–crRNA–Csx29 complex. (**B**) Interface between Cas7-11 and Csx29 in the Cas7-11–crRNA–Csx29 complex. The Cas11 and INS domains are omitted for clarity. (**C**) Location of the Csx29 active site. The catalytic residue H615 of the Csx29 protease is colored red. (**D** and **E**) Interfaces between Cas7-11 and Csx29 in Cas7-11–crRNA–Csx29 (D) and Cas7-11–crRNA–Csx29–tgRNA (E). Csx29 is shown as a surface representation, except for the AR, which is shown as a ribbon representation. The AR and APD are disordered in the Cas7-11–crRNA–Csx29–tgRNA structure in (E).

β-hairpin) and Cas7.2 (ZF) (Fig. 2B). TPR3 to TPR7 do not contact Cas7-11. The CHAT protease domain of Csx29 interacts with Cas7.1 (thumb-like β-hairpin), Cas7.2 (ZF), Cas7.3 (ZF), and L2 of Cas7-11 (Fig. 2B and fig. S7A). The protease active site of Csx29 is near the Cas7.2 domain of Cas7-11 (Fig. 2C), suggesting limited accessibility for the peptide substrate in this conformation. Furthermore, in contrast to the separase–securin structure (*17*), the side chain of the catalytic residue C658 is buried inside the CHAT domain in the present structure (fig. S6), indicating that a structural rearrangement of C658 would be required for the substrate cleavage. These observations suggest that the Cas7-11–crRNA–Csx29 structure represents the inactive state of the Csx29 putative protease.

Downloaded from https://www.science.org at Shanghai Normal University on November 25, 2022

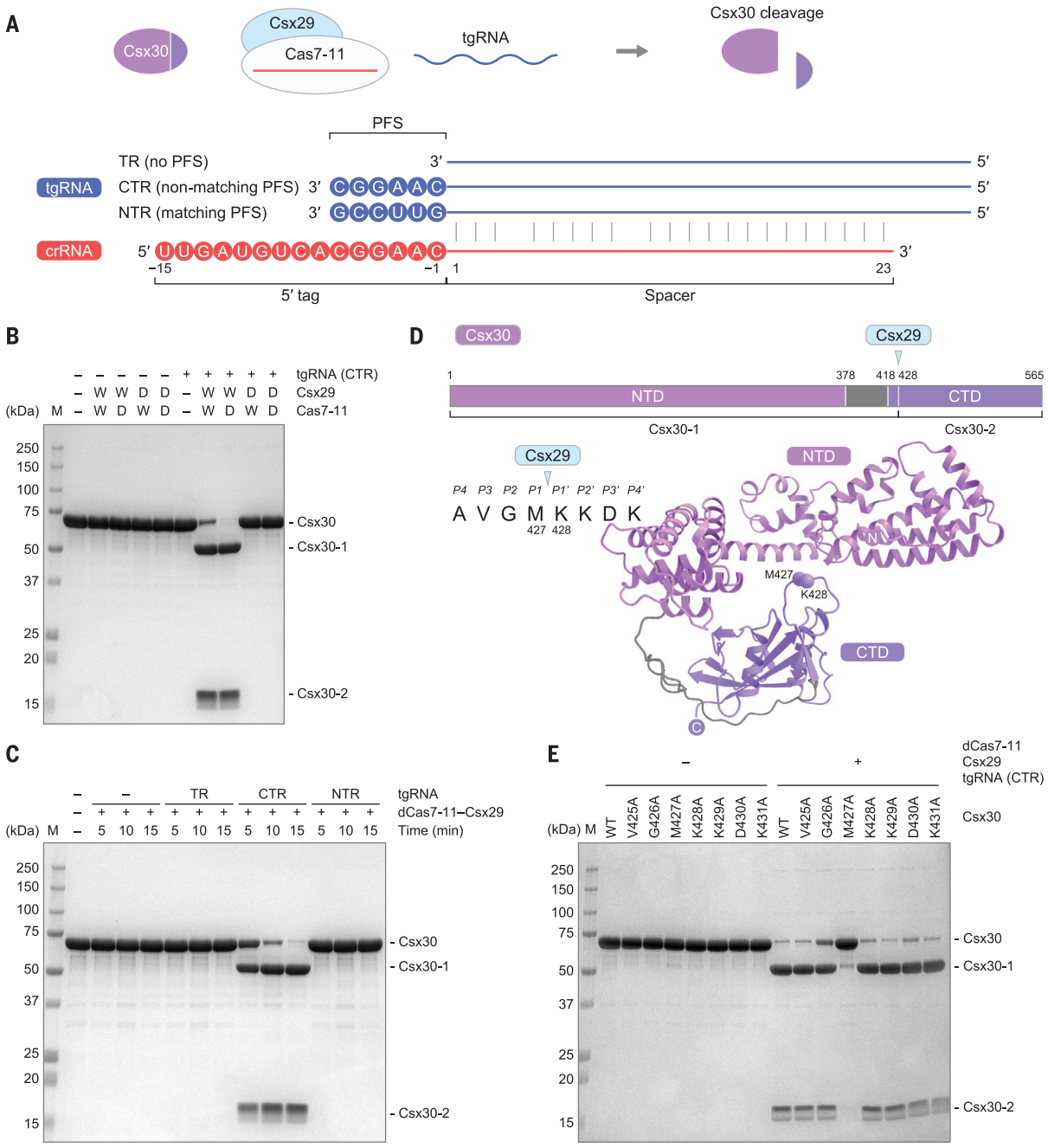


Fig. 3. tgRNA-triggered Csx30 cleavage by Csx29. (**A**) Schematic of the RNA-triggered Csx30 cleavage by the Cas7-11–crRNA–Csx29 complex. TR, tgRNA without a PFS; CTR, cognate tgRNA with a nonmatching PFS; NTR, noncognate tgRNA with a matching PFS. (**B**) RNA-triggered Csx30 cleavage by the Cas7-11–crRNA–Csx29 complex. The Cas7-11–crRNA–Csx29 complex was incubated with Csx30 at 37°C for 10 min in the presence or absence of the tgRNA (CTR). The wild-type (W) and catalytically deactivated (D) versions of Cas7-11 and Csx29 were used. (**C**) Effects of the complementarity between the crRNA 5′ tag and tgRNA PFS on the Csx30 cleavage. The dCas7-11–crRNA–Csx29 complex was incubated with Csx30 at 37°C for 5, 10, or 15 min in the presence of the tgRNA (TR, CTR, or NTR). (**D**) Proteolytic cleavage site in Csx30. The Csx30 site cleaved by Csx29 is indicated by a triangle. The Csx30 structure was predicted using AlphaFold2 (*18*), and the Cα atoms of M427 and K428 at the cleavage site are indicated by spheres. (**E**) Csx29-mediated cleavage of the Csx30 mutants. The dCas7-11–crRNA–Csx29 complex was incubated with the Csx30 mutants at 37°C for 10 min, in the presence or absence of the tgRNA (CTR). In (B), (C), and (E), the proteins were analyzed by SDS-polyacrylamide gel electrophoresis, and the gel was stained with Coomassie brilliant blue.

tgRNA binding–induced structural change in the Cas7-11–Csx29 complex

Comparison of the Cas7-11–crRNA–Csx29 structures with and without the tgRNA revealed different Csx29 conformations (Fig. 2, D and E, and movie S2). In the tgRNA-free structure, TPR1 and TPR2 of Csx29 interact with Cas7.3 and Cas7.1/Cas7.2 of Cas7-11, respectively (Fig. 2, B and D, and fig. S9A). By contrast, in the tgRNA-bound structure, TPR1 and TPR2 of Csx29 are farther away from Cas7-11 and do not interact with Cas7.1–Cas7.3 of Cas7-11 because of the binding of the tgRNA 3′ region between Cas7-11 and Csx29 (Fig. 2E and fig. S9B). In the 6-nt protospacer flanking sequence (PFS) of the tgRNA, only C(−1) and A(−2) are well resolved in the density map and interact with Cas7-11 (L2/Cas7.3) and Csx29 (TPR1/TPR2)

Downloaded from https://www.science.org at Shanghai Normal University on November 25, 2022

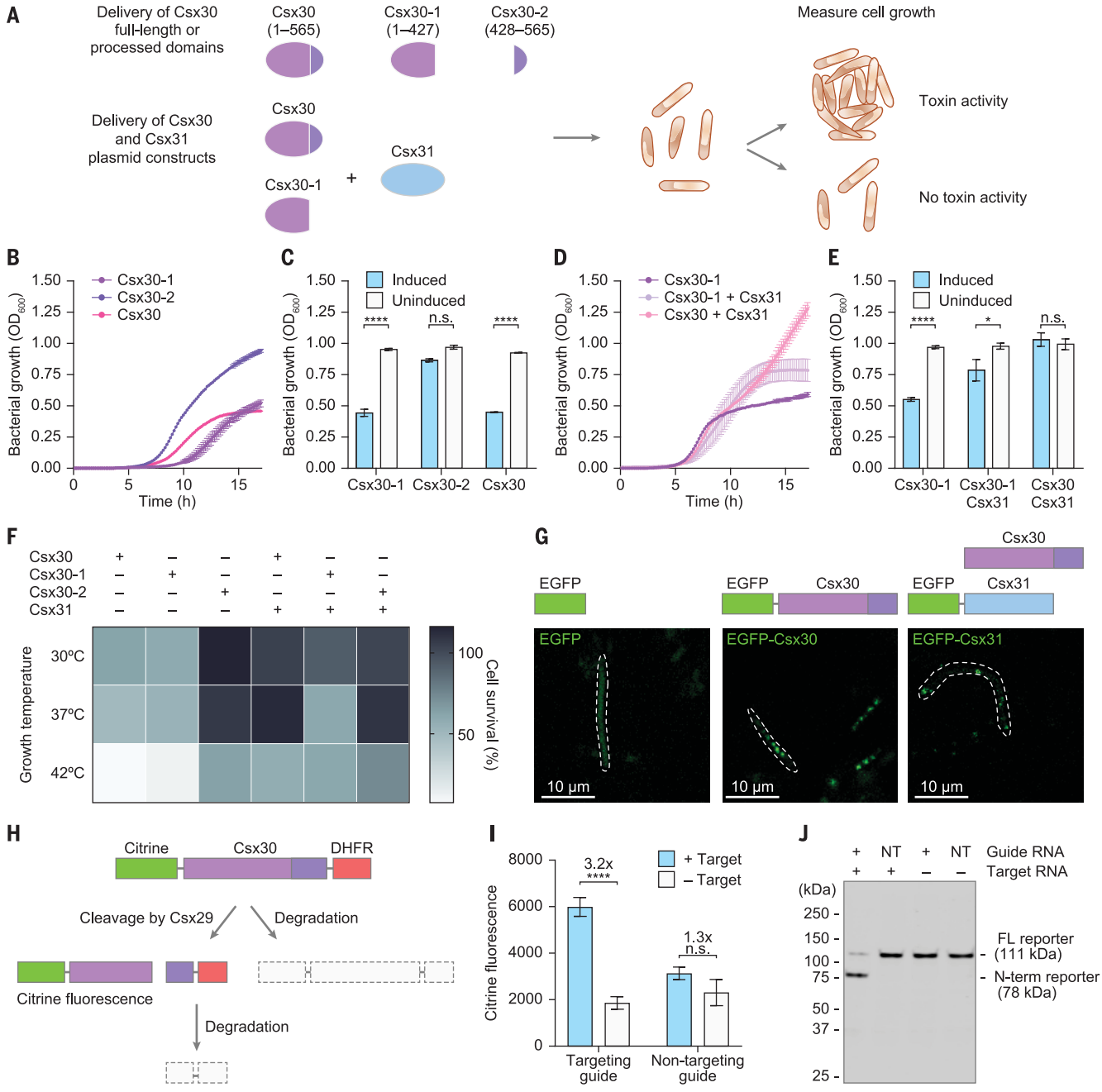


Fig. 4. Effects of Csx30 and Csx31 on bacterial cell growth. (**A**) Schematic of bacterial growth assays for studying the Csx30 and Csx31 functions. (**B** and **C**) Growth curves (B) and end-point analyses (C) of *E. coli* expressing full-length Csx30, the N-terminal fragment (residues 1 to 427) of Csx30 (Csx30-1), or the C-terminal fragment (residues 428 to 565) of Csx30 (Csx30-2). (**D** and **E**) Growth curves (D) and end-point analyses (E) of *E. coli* expressing Csx30-1, full-length Csx30 and Csx31, or Csx30-1 and Csx31. In (B) to (E), growth was compared between induced and uninduced expression conditions. In (C) and (E), significance was calculated by two-tailed Student's *t* test (****$P < 0.0001$; n.s., not significant). Data are shown as mean ± SEM ($n = 3$). (**F**) Heatmap comparing the survival percentages of bacteria expressing Csx30-1, Csx30-2, full-length Csx30 and Csx31, full-length Csx30 alone, Csx30-1 and Csx31, or Csx30-2 and Csx31, cultured at three different temperatures. Percent survival was calculated by the ratio of optical density at 600 nm (OD_{600}) of the bacterial culture under the induced conditions over the OD_{600} for the noninduced conditions. Color scale shows percent survival from 0 to 100%. (**G**) Confocal images of *E. coli* expressing EGFP alone, EGFP-Csx30, or EGFP-Csx31 and unlabeled Csx30. White outlines indicate the shapes of individual *E. coli* cells. (**H**) Schematic of the mammalian application of the Cas7-11–Csx29–Csx30 degron reporter system for RNA sensing in live cells. (**I**) Citrine fluorescence of HEK293FT cells transfected with either the Gluc target or pUC19 control target in the presence of the Cas7-11–Csx29–Csx30 degron reporter. Significance was calculated with two-tailed Student's *t* test (****$P < 0.0001$). Data are shown as mean ± SEM ($n = 3$). (**J**) RNA-triggered Csx30 reporter cleavage in HEK293FT cells. The N-terminally FLAG-tagged citrine–Csx30–degron reporter was transfected either with or without the Gluc target and with a targeting or nontargeting (NT) guide. Forty-eight hours after transfection, total protein was extracted from the transfected HEK293FT cells and analyzed by Western blot with an anti-FLAG antibody.

Downloaded from https://www.science.org at Shanghai Normal University on November 25, 2022

(fig. S9, B and C). The nucleobases C(−1) and A(−2) stack with R375 (L2) and Y718 (Cas7.3), respectively (fig. S9, B and C). In addition, the phosphate groups between A(−3) and A(−2) and between A(−2) and C(−1) interact with R131 (TPR2) and R145 (TPR2), respectively (fig. S9B). These interactions induce a kink turn between A(−2) and C(−1) in the PFS, thereby projecting the tgRNA nucleotides downstream of position −2 toward the AR of Csx29.

There are also structural differences in the AR–APD of Csx29 between the RNA-free and RNA-bound structures. Whereas the AR extensively interacts with TPR1 to TPR5 and APD in the tgRNA-free structure (Fig. 2D and fig. S9A), the AR-APD of Csx29 is not resolved in the density map in the tgRNA-bound structure (Fig. 2E and fig. S3B). In addition, the pseudoprotease domain of Csx29 in the tgRNA-bound structure exhibits weaker density compared with that in the tgRNA-free structure (fig. S3, A and B). These observations suggest that tgRNA binding increases the conformational flexibility of the CHAT protease domain of Csx29, and this conformational change releases the steric block of the Csx29 active site, allowing access to the substrate protein. Structural comparisons between the two Cas7-11–Csx29 complexes suggest steric clash between the tgRNA PFS and the Csx29 AR (fig. S9D), highlighting the importance of the PFS for the tgRNA-induced conformational change in Csx29. These structural observations indicate that Csx29 is a tgRNA-triggered protease.

tgRNA-triggered Csx30 cleavage by Csx29

Given that Csx30 and Csx31 are encoded together with Cas7-11 and Csx29 in the *D. ishimotonii* CRISPR locus and are highly conserved among the type III-E systems (*8*), we hypothesized that Csx29 could target either Csx30 or Csx31. To test this hypothesis, we attempted to prepare the recombinant Csx30 and Csx31 proteins and determine whether they are cleaved by Csx29 in a tgRNA-dependent manner. Csx30 was purified as a soluble protein, whereas Csx31 was expressed in an insoluble fraction. We examined the in vitro cleavage of Csx30 by Cas7-11–crRNA–Csx29 in the absence and presence of the tgRNA, and found that Cas7-11–crRNA–Csx29 cleaved Csx30 into two fragments, Csx30-1 (~50 kDa) and Csx30-2 (~15 kDa), only in the presence of the tgRNA (Fig. 3, A and B).

The H615A/C658A mutations in Csx29 abolished the Csx30 cleavage (Fig. 3B) but did not affect the tgRNA cleavage by Cas7-11 (fig. S10A), indicating the separable nuclease and protease activities. Furthermore, the D429A/D654A catalytic mutations in Cas7-11 abolished tgRNA cleavage (fig. S10A), as previously observed (*12*), and, unexpectedly, improved the Csx30 cleavage by Csx29 (Fig. 3B and fig. S10B). This improvement in the proteolytic activity suggests that the tgRNA dissociates from the effector complex after the Cas7-11–mediated cleavage, and that the Csx29 protease is only active when a tgRNA is bound to the Cas7-11–Csx29 complex. Thus, Csx30 is cleaved by the CHAT protease domain of Csx29 in a tgRNA-dependent manner.

The base complementarity between the crRNA 5′ tag and a tgRNA PFS regulates the activities of the type III-A Csm effector complex to avoid an autoimmune response in the type III-A system (*13*, *14*). Thus, we examined the effects of the PFS in the tgRNA on Csx30 cleavage using a tgRNA without a PFS, a cognate tgRNA with a nonmatching PFS, or a noncognate tgRNA with a matching PFS (Fig. 3A). Csx30 was cleaved by the Cas7-11–Csx29 complex efficiently in the presence of cognate tgRNA with a nonmatching PFS, but not the tgRNA without a PFS or the noncognate tgRNA with a matching PFS (Fig. 3C), consistent with our observation that a nonmatching PFS plays a role in the structural changes and protease activation of Csx29. These findings suggest a potential mechanism for self-targeting avoidance in the type III-E system, as in the type III-A system.

The N-terminal analysis of the Csx30-2 fragment showed that it begins with K428 (fig. S11), demonstrating that Csx30 is cleaved by Csx29 between M427 and K428 (Fig. 3D). Structure prediction using AlphaFold2 (*18*) indicated that Csx30 consists of an NTD and a C-terminal domain (CTD), which are connected by a linker region. The NTD (residues 1 to 377) contains two α-helical subdomains, whereas the CTD (residues 418 to 565) comprises a core β-barrel with flanking α helices (Fig. 3D). The cleavage site between M427 and K428 is located in a β-hairpin within the Csx30 CTD (Fig. 3D). We examined the in vitro Csx29-mediated cleavage of eight Csx30 mutants, in which residues V425 to K431 were individually replaced with alanine. The M427A and G416A substitutions substantially and slightly reduced the Csx30 cleavage, respectively, whereas the other substitutions had almost no effect (Fig. 3E). Accordingly, Csx29 seems to primarily recognize M427 at the P1 site within the AVGM|KKDK sequence in Csx30 and cleaves Csx30 between M427 (P1) and K428 (P1′). Thus, the Cas7-11–Csx29 complex catalyzes the tgRNA-triggered proteolysis of Csx30.

Effects of Csx30 and Csx31 on bacterial cell growth

To explore the physiological relevance of the Csx29-mediated Csx30 cleavage, we overexpressed the full-length Csx30 (referred to as Csx30 for simplicity), the N-terminal fragment of Csx30 (residues 1 to 427, Csx30-1), or the C-terminal fragment of Csx30 (residues 428 to 565, Csx30-2) in *Escherichia coli*, and monitored the cell growth (Fig. 4A). Overexpression of Csx30 substantially inhibited cell growth compared with uninduced controls (Fig. 4, B and C, and fig. S12, A and B). Overexpression of Csx30-1 similarly caused pronounced growth suppression, whereas Csx30-2 displayed only mild inhibition (Fig. 4, B and C, and fig. S12, A and B), indicating that Csx30-1 is necessary and sufficient for the observed growth effects of the full-length Csx30. Because the AlphaFold2 structural prediction (*18*) suggested that Csx30 and Csx31 have oppositely charged surfaces and could electrostatically interact with each other (fig. S12C), we also explored the effect of Csx31 on bacterial growth. Overexpression of Csx31 rescued the Csx30-mediated growth defect, but could not completely eliminate the Csx30-1–induced growth suppression (Fig. 4, D and E, and fig. S12, B and D). These data indicate that Csx31 interacts with Csx30 and regulates Csx30-induced growth suppression, whereas the generation of the Csx30-1 and Csx30-2 fragments by the Cas7-11–Csx29 protease interferes with this regulation.

Interactions among Csx30, Csx31, and RpoE

The common co-occurrence of Cas7-11, Csx30, Csx31, and the stress-associated sigma factor RpoE (*19*) in type III-E CRISPR loci (*2*, *8*) suggests interplay among these four proteins, such that the observed Csx30-induced growth suppression might be caused by interactions with endogenous *E. coli* RpoE (EcRpoE). Given the involvement of EcRpoE in cellular heat shock responses (*20*, *21*), we hypothesized that the growth defects might be more pronounced at higher temperatures because of the inhibition of EcRpoE by Csx30 and Csx31, and tested the effects of Csx30 and Csx31 in *E. coli* at temperatures ranging from 30° to 42°C. In agreement with our hypothesis, the growth suppression by Csx30 was stronger at higher temperatures across all tested combinations (Fig. 4F), implicating EcRpoE in the growth defects caused by the overexpression of Csx30 and Csx31.

To examine the direct interactions among Csx30, Csx31, and *D. ishimotonii* RpoE (DiRpoE), we coexpressed the three proteins in *E. coli* and analyzed complex formation by gel-filtration chromatography. Csx30, Csx31, and DiRpoE eluted as a single peak (fig. S13A), indicating that they form a stable complex. Like the isolated Csx30, Csx30 in the Csx30–Csx31–DiRpoE complex was cleaved by Cas7-11–Csx29, and Csx30-1, Csx31, and DiRpoE co-eluted from the column (fig. S13B), indicating that Csx30-1, Csx31, and RpoE remain complexed after Csx30 cleavage, whereas Csx30-2 dissociates from the complex. Consistently, structural prediction implied that Csx30, Csx31, and DiRpoE form a ternary complex in which the Csx30 NTD extensively interacts with DiRpoE (fig. S13C). DiRpoE is structurally similar to EcRpoE (fig. S13D), suggesting that the observed cell

Downloaded from https://www.science.org at Shanghai Normal University on November 25, 2022

growth inhibition could be mediated through Csx30–EcRpoE interactions, similar to the mechanism of the anti-sigma factor RseA (*22*). However, *D. ishimotonii* lacks RseA homologs (*23*), so DiRpoE probably mediates the transcriptional response through distinct mechanisms that remain to be characterized. A Dali search (*16*) revealed structural similarity between the Csx30 CTD and pore-forming proteins in type IV secretion systems, such as CagX (*24*) (fig. S13E). Given the reduced growth effects of full-length Csx30 in *E. coli* compared with Csx30-1, the Csx30 CTD might function as a membrane anchor rather than as a pore-forming protein, consistent with the role of the membrane-localized RseA (*19*, *23*). The CTD and NTD of Csx30 are connected through a flexible linker, suggesting that the Csx29-mediated cleavage releases the N-terminal fragment of Csx30 (Csx30-1) into the cytoplasm, thereby modulating gene expression through RpoE suppression. Csx30 NTDs are highly conserved (fig. S14), whereas Csx30 CTDs are divergent and can be divided into seven distinct groups (fig. S15), of which two are homologous protein domains found in other contexts. One is an uncharacterized DUF4384 family member that is often fused to different proteases (*25*). The other CTD is similar to the pilus assembly protein PilP, which forms a periplasmic ring of bacterial type IV pili (*26*). These observations highlight the mechanistic diversity of the Csx30-mediated RpoE interactions and programmed gene expression modulation.

Localization of Csx30 and Csx31 in bacterial cells

To explore the growth suppression associated with the expression of Csx30, the putative membrane localization of the Csx30 CTD, and the corresponding regulatory function of Csx31, we imaged Csx30 and Csx31 by fusing bacterial codon-optimized enhanced GFP (EGFP) to the N termini of both proteins. Protein localization in *E. coli* transformed with a plasmid expressing EGFP-Csx30, plasmids expressing EGFP-Csx31 and unlabeled Csx30, or a plasmid expressing EGFP alone was imaged. Both labeled Csx30 alone and labeled Csx31 co-expressed with Csx30 localized to individual foci, whereas EGFP diffused throughout the cells (Fig. 4G). These results suggest the direct interaction between Csx30 and Csx31 through colocalization at foci in bacterial cells before Csx29-mediated Csx30 cleavage.

Engineering Csx29 and Csx30 for programmable RNA sensing in mammalian cells

The programmable transcript-activated protease activity of the Cas7-11–Csx29–Csx30 system could enable multiple applications in mammalian cells, including transcript sensing. We codon-optimized Cas7-11, Csx29, and Csx30 for mammalian cells and placed the Csx30 protein sequence between a citrine protein and a dihydrofolate reductase (DHFR) degron (*27*), which would eliminate citrine fluorescence unless Csx30 was cleaved by Cas7-11–Csx29 because of the sequence-specific recognition of a target sequence (Fig. 4H). We transfected human embryonic kidney (HEK) 293FT cells with either a targeting or nontargeting guide RNA toward a Gaussia luciferase (Gluc) target to test the activation of the Cas7-11–Csx29–Csx30 system. In the presence of the Gluc mRNA target, we observed threefold higher citrine fluorescence with the targeting, but not nontargeting, guide RNA (Fig. 4I), indicating that Csx29 is activated and cleaves the DHFR degron from the citrine reporter. To validate that the increase in citrine fluorescence was caused by the cleavage of Csx30 in the reporter, we analyzed the total protein from the HEK293FT cells by Western blot using an anti-FLAG antibody and visualized the N-terminally FLAG-tagged reporter. The molecular mass of the reporter protein decreased from ~110 to 78 kDa only in the presence of the tgRNA and targeting guide, indicating the Csx29-mediated cleavage of Csx30 in the reporter (Fig. 4J and fig. S16). These results demonstrate that the Cas7-11–Csx29–Csx30 system is reprogrammable in mammalian cells and can be used as a protease-based RNA-guided posttranslational sensor.

Discussion

Our structural and functional analyses of the type III-E CRISPR-Cas systems revealed notable complexity and fine-tuned regulation. The effects of Csx30 and Csx31 on bacterial growth suggested that Csx29-mediated Csx30 cleavage releases the N-terminal fragment of Csx30 bound to Csx31, inhibiting host cell growth (fig. S17). Furthermore, our biochemical and structural analyses indicated that Csx30, Csx31, and RpoE can form a ternary complex in which Csx30 extensively interacts with RpoE, suggesting that RpoE inhibition by Csx30 contributes to the observed cell growth arrest, akin to the Cas13 collateral activity-based cell growth arrest (*28*). Csx30 cleavage by Csx29 could also facilitate the dissociation of RpoE from Csx30, allowing RpoE to engage in a transcriptional response to viral infection. By leveraging the programmable nature of this system, we developed a molecular RNA sensor for transcripts in mammalian cells, demonstrating the potential of this Cas7-11–Csx29–Csx30 system for sensing and therapeutic applications, analogous to recently developed mammalian RNA sensors (*29*, *30*).

Thus, in type III-E CRISPR-Cas systems, the Cas7-11–Csx29 effector complex likely degrades the ssRNA transcripts of phage genes and stimulates potentially toxic host cell stress responses through the Csx29-mediated Csx30 cleavage (fig. S17). This type of programmed growth suppression, through cell death or growth arrest, appears analogous to that caused by gasdermins, the bacterial membrane pore-forming toxins that are switched on by the release of auto-inhibitory peptides by associated proteases that become activated during phage infection (*31*, *32*). Moreover, given the high diversity of Csx30 CTDs (fig. S15), further explorations of other subtype III-E systems might reveal additional functions associated with Cas7-11–mediated tgRNA recognition.

Among the CRISPR-Cas systems, a biological, if not mechanistic, analogy can be found in the type VI systems, where the Cas13–crRNA effector complex recognizes complementary phage mRNAs and cleaves both phage (specifically and in *cis*) and host (indiscriminately and in *trans*) transcripts, thus stalling cell growth and with it the infectious cycle (*28*). Similarly, in some type III systems, the CRISPR-Lon protease is activated by cyclic oligoadenylates upon RNA recognition by the effector complexes and cleaves the associated CRISPR-T protein specifically, releasing a toxic fragment (*33*). Our characterization of the subtype III-E system highlights the remarkable diversity of CRISPR-associated functions activated by programmable nucleic acid recognition, motivating continued exploration of CRISPR-associated proteins and their programmable functions that could be useful for biological applications. Our findings that the type III-E Cas7-11–Csx29 effector complex is an RNA-triggered nuclease-protease establish a distinct paradigm of prokaryotic signal transduction in viral immunity and could pave the way for the development of new RNA/protein-targeting technologies, including in vitro diagnostics and cellular RNA sensing.

REFERENCES AND NOTES

1. F. Hille *et al.*, *Cell* **172**, 1239–1259 (2018).
2. K. S. Makarova *et al.*, *Nat. Rev. Microbiol.* **18**, 67–83 (2020).
3. M. Kazlauskiene, G. Kostiuk, Č. Venclovas, G. Tamulaitis, V. Siksnys, *Science* **357**, 605–609 (2017).
4. O. Niewoehner *et al.*, *Nature* **548**, 543–548 (2017).
5. C. Rouillon, J. S. Athukoralage, S. Graham, S. Grüschow, M. F. White, *eLife* **7**, e36734 (2018).
6. W. Han, S. Pan, B. López-Méndez, G. Montoya, Q. She, *Nucleic Acids Res.* **45**, 10740–10750 (2017).
7. A. R. VanderWal, J.-U. Park, B. Polevoda, E. H. Kellogg, M. R. O'Connell, CRISPR-Csx28 forms a Cas13b-activated membrane pore required for robust CRISPR-Cas adaptive immunity. bioRxiv 466367 [Preprint] (2021); https://doi.org/10.1101/2021.11.02.466367.
8. A. Özcan *et al.*, *Nature* **597**, 720–725 (2021).
9. S. P. B. van Beljouw *et al.*, *Science* **373**, 1349–1353 (2021).
10. O. O. Abudayyeh *et al.*, *Nature* **550**, 280–284 (2017).
11. J. S. Gootenberg *et al.*, *Science* **356**, 438–442 (2017).
12. K. Kato *et al.*, *Cell* **185**, 2324–2337.e16 (2022).
13. L. You *et al.*, *Cell* **176**, 239–253.e16 (2019).
14. N. Jia *et al.*, *Mol. Cell* **73**, 264–277.e5 (2019).
15. N. Zeytuni, R. Zarivach, *Structure* **20**, 397–405 (2012).
16. L. Holm, *Methods Mol. Biol.* **2112**, 29–42 (2020).
17. J. Yu *et al.*, *Nature* **596**, 138–142 (2021).
18. J. Jumper *et al.*, *Nature* **596**, 583–589 (2021).
19. L. Connolly, A. De Las Penas, B. M. Alba, C. A. Gross, *Genes Dev.* **11**, 2012–2021 (1997).

Downloaded from https://www.science.org at Shanghai Normal University on November 25, 2022

20. J. Mecsas, P. E. Rouviere, J. W. Erickson, T. J. Donohue, C. A. Gross, *Genes Dev.* **7** (12b), 2618–2628 (1993).
21. K. Hiratsu, M. Amemura, H. Nashimoto, H. Shinagawa, K. Makino, *J. Bacteriol.* **177**, 2918–2922 (1995).
22. E. A. Campbell *et al*., *Mol. Cell* **11**, 1067–1078 (2003).
23. V. Schnaars *et al*., *Microb. Physiol.* **31**, 1–20 (2021).
24. J. M. Chung *et al*., *eLife* **8**, e47644 (2019).
25. S. Lu *et al*., *Nucleic Acids Res.* **48**, D265–D268 (2020).
26. Y.-W. Chang *et al*., *Science* **351**, aad2001 (2016).
27. X. J. Gao, L. S. Chong, M. S. Kim, M. B. Elowitz, *Science* **361**, 1252–1258 (2018).
28. A. J. Meeske, S. Nakandakari-Higa, L. A. Marraffini, *Nature* **570**, 241–245 (2019).
29. K. Jiang *et al*., *Nat. Biotechnol.* 10.1038/s41587-022-01534-5 (2022).
30. E. M. Zhao *et al*., *Nat. Biotechnol.* **40**, 539–545 (2022).
31. A. G. Johnson *et al*., *Science* **375**, 221–225 (2022).
32. C. Clavé *et al*., *Proc. Natl. Acad. Sci. U.S.A.* **119**, e2109418119 (2022).
33. C. Rouillon *et al*., SAVED by a toxin: Structure and function of the CRISPR Lon protease. bioRxiv 471393 [Preprint] (2021); https://doi.org/10.1101/2021.12.06.471393.

ACKNOWLEDGMENTS

We thank M. Hiraizumi and the staff scientists at The University of Tokyo's cryo-EM facility, especially Y. Sakamaki, for help with cryo-EM data collection, and N. Okumura for help with the N-terminal analysis. **Funding:** S.A. is supported by the Japan Society for the Promotion of Science (JSPS) (KAKENHI grant 21H05736). K.S.M. and E.V.K are supported through the National Institutes of Health's (NIH's) Intramural Research Program (National Library of Medicine). H.N. is supported by the Platform Project for Supporting Drug Discovery and Life Science Research Basis for Supporting Innovative Drug Discovery and Life Science Research (BINDS) from the Japanese Agency for for Medical Research and Development (AMED) (grant JP21am0101115 support number 2792 and grant JP21wm0325048h0001), JSPS (KAKENHI grants 20K20579 and 21H05281), the Takeda Medical Research Foundation, and the Inamori Research Institute for Science. J.S.G. and O.O.A. are supported by the NIH (grants 1R21-AI149694, R01-EB031957, and R56-HG011857), the McGovern Institute Neurotechnology (MINT) program; the K. Lisa Yang and Hock E. Tan Center for Molecular Therapeutics in Neuroscience, the G. Harold & Leila Y. Mathers Charitable Foundation, the MIT John W. Jarve (1978) Seed Fund for Science Innovation, FastGrants, the Cystic Fibrosis Foundation, Google Ventures, by a Longevity Impetus Grant from the Norn Group, the NHGRI/TDCC Opportunity Fund, and the McGovern Institute. **Author contributions:** Conceptualization: K.K., O.O.A., J.S.G., H.N.; Funding acquisition: O.O.A., J.S.G., H.N.; Investigation: K.K., S.O., C.S., K.J., W.Z., J.I., Y.I., S.A., T.N., K.S.M., E.V.K., O.O.A., J.S.G., H.N.; Supervision: O.O.A., J.S.G., H.N.; Writing – original draft: K.K., C.S., K.J., O.O.A., J.S.G., H.N.; Writing – review and editing: E.V.K., O.O.A., J.S.G., H.N. **Competing interests:** The authors have filed a patent application related to this work. J.S.G. and O.O.A. are co-founders of Sherlock Biosciences, Proof Diagnostics, Moment Biosciences, and Tome Biosciences. H.N. is an adviser for Moment Biosciences. **Data and materials availability:** Relevant plasmids are available from the corresponding authors under a material transfer agreement with MIT or Addgene. The EM densities have been deposited in the Electron Microscopy Data Bank under the accession codes 33695 and 34218. The model coordinates have been deposited in the Protein Data Bank under the accession codes 7Y7X and 8GS2. **License information:** Copyright © 2022 the authors, some rights reserved; exclusive licensee American Association for the Advancement of Science. No claim to original US government works. https://www.science.org/about/science-licenses-journal-article-reuse

SUPPLEMENTARY MATERIALS

science.org/doi/10.1126/science.add7347
Materials and Methods
Figs. S1 to S17
Tables S1 to S2
References (*34*–*49*)
MDAR Reproducibility Checklist
Movies S1 and S2

View/request a protocol for this paper from *Bio-protocol*.

Submitted 30 June 2022; accepted 24 October 2022
10.1126/science.add7347

Downloaded from https://www.science.org at Shanghai Normal University on November 25, 2022

Science

RNA-triggered protein cleavage and cell growth arrest by the type III-E CRISPR nuclease-protease

Kazuki KatoSae OkazakiCian Schmitt-UlmsKaiyi JiangWenyuan ZhouJunichiro IshikawaYukari IsayamaShungo AdachiTomohiro NishizawaKira S. MakarovaEugene V. KooninOmar O. AbudayyehJonathan S. GootenbergHiroshi Nishimasu

Science, 378 (6622), • DOI: 10.1126/science.add7347

Two enzymes in one

Apart from their RNA-guided nuclease activity, CRISPR systems encompass multiple accessory proteins that enhance or modulate immune functions. Kato *et al*. found that type III-E CRISPR systems include the caspase-like protease Csx29, which cleaves another accessory protein, Csx30, when activated upon target RNA recognition by Cas7-11. This cleavage yields toxic Csx30 fragments that presumably inhibit the specialized sigma factor RpoE, modulate bacterial response to infection, and cause bacterial growth arrest, thereby abrogating phage infection. These findings expand the known complexity of CRISPR immune responses and enable the engineering of protease-based programmable RNA sensing in mammalian cells. —DJ

View the article online
https://www.science.org/doi/10.1126/science.add7347
Permissions
https://www.science.org/help/reprints-and-permissions

Downloaded from https://www.science.org at Shanghai Normal University on November 25, 2022

Use of this article is subject to the Terms of service

Science (ISSN) is published by the American Association for the Advancement of Science. 1200 New York Avenue NW, Washington, DC 20005. The title *Science* is a registered trademark of AAAS.
Copyright © 2022 The Authors, some rights reserved; exclusive licensee American Association for the Advancement of Science. No claim to original U.S. Government Works